

pubs.acs.org/jmc Article

Photocytotoxicity of Thiophene- and Bithiophene-Dipicolinato Luminescent Lanthanide Complexes

Carime V. Rodrigues, Katherine R. Johnson, Vincent C. Lombardi, Marcelo O. Rodrigues, Josiane A. Sobrinho, and Ana de Bettencourt-Dias*



Cite This: J. Med. Chem. 2021, 64, 7724–7734



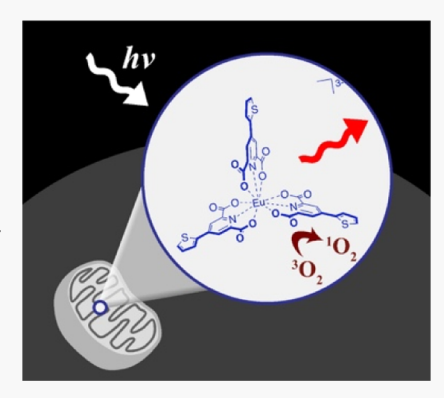
ACCESS

Metrics & More



s Supporting Information

ABSTRACT: New thiophene-dipicolinato-based compounds, K_2nTdpa (n=1,2), were isolated. Their anions are sensitizers of lanthanide ion (Ln^{III}) luminescence and singlet oxygen generation ($^{\rm I}O_2$). Emission in the visible and near-infrared regions was observed for the Ln^{III} complexes with efficiencies (ϕ^{Ln}) $\phi^{Eu}=33\%$ and $\phi^{Yb}=0.31\%$ for $1Tdpa^{2-}$ and $\phi^{Yb}=0.07\%$ for $2Tdpa^{2-}$. The latter does not sensitize Eu^{III} emission. Fluorescence imaging of HeLa live cells incubated with $K_3[Eu(1Tdpa)_3]$ indicates that the complex permeates the cell membrane and localizes in the mitochondria. All complexes generate 1O_2 in solution with efficiencies ($\phi_{^1O_2}$) as high as 13 and 23% for the Gd^{III} complexes of $1Tdpa^{2-}$ and $2Tdpa^{2-}$, respectively. $[Ln(nTdpa)_3]^{3-}$ (n=1,2) are phototoxic to HeLa cells when irradiated with UV light with IC_{50} values as low as 4.2 μ M for $[Gd(2Tdpa)_3]^{3-}$ and 91.8 μ M for $[Eu(1Tdpa)_3]^{3-}$. Flow cytometric analyses indicate both apoptotic and necrotic cell death pathways.



■ INTRODUCTION

Singlet oxygen ($^{1}O_{2}$) is a reactive oxygen species directly linked to tissue damage and cellular death. 1 $^{1}O_{2}$ -generating photosensitizers are useful in photodynamic therapy (PDT), a cancer treatment option that uses light to excite photosensitizers to generate $^{1}O_{2}$ within diseased cells, resulting in cell death. PDT is minimally invasive with reduced patient pain, short recovery times, and a lower likelihood of infection.

Porfimer sodium, or Photofrin, is a porphyrin-based photosensitizer that was approved by the U.S. Food and Drug Administration in 1993 for the treatment of bladder cancer and has since been approved for several other cancers, including endobronchial and esophageal cancers.³⁻⁵ Porphyrin-based compounds are among the most studied photosensitizers for PDT.6,7 While efficient, several of the compounds include a toxic heavy metal to promote intersystem crossing (ISC) for more efficient ¹O₂ generation.⁸ In addition, many show poor solubility, aggregation, which shortens the lifetime of the excited state resulting in lower ¹O₂ generation quantum yields, ^{10,11} and high dark toxicity, which limits dosage concentration. ^{12,13} More recent work highlights the progress made in the development of improved photosensitizers, with complexes of Ru^{II}, Pd^{II}, and Pt^{II} with triplet excited states appropriately positioned to promote the formation of ${}^{1}O_{2}$. However, while these compounds are promising, ruthenium, palladium, and platinum are costly rare metals.¹⁹ Thus, there is a fundamental interest in the development of new types of efficient ¹O₂ generators.

Ideal photosensitizers for PDT need to be effective at low doses, and those with built-in multifunctional capabilities show

a distinct advantage.²⁰ The additional ability to luminesce is one such example as it provides imaging and tracking ability in solution or within biological tissues. This allows researchers to study the compound's mechanism of action.²¹ Bioimaging can be accomplished with lanthanide ion (LnIII) complexes, as the metal ions, which are less costly than other metals used as photosensitizers, 19 have unique luminescence properties. They emit light due to parity-forbidden 4f-4f transitions. Because the 4f orbitals are shielded by the 5s and 5p, the f-f transitions are not drastically affected by the coordination environment. Thus, these ions are attractive for bioimaging applications, as they display long luminescence decay lifetimes, narrow, metalspecific emission bands, and large Stokes shifts of sensitized emission (vide infra), which enable time-gated luminescence imaging with resulting increased signal-to-noise ratio, making it easier to discriminate the metal-centered emission from biofluorescence. 22,23

Since the transitions are forbidden, the promotion of metalcentered emission is more easily achieved through coordinated sensitizers, or antennae, in a process referred to as the antenna effect.²⁴ The sensitizer (ligand or antenna) absorbs a photon, and through a sequence of energy transfer (ET) steps, the emissive excited state of the Ln^{III} is populated, as illustrated in

Received: March 10, 2021 Published: May 21, 2021





Figure 1. In addition, the triplet (³T) state of the sensitizer, which is directly involved in the population of the emissive state, can transfer energy to O₂ to generate cytotoxic ¹O₂. ^{24,25}

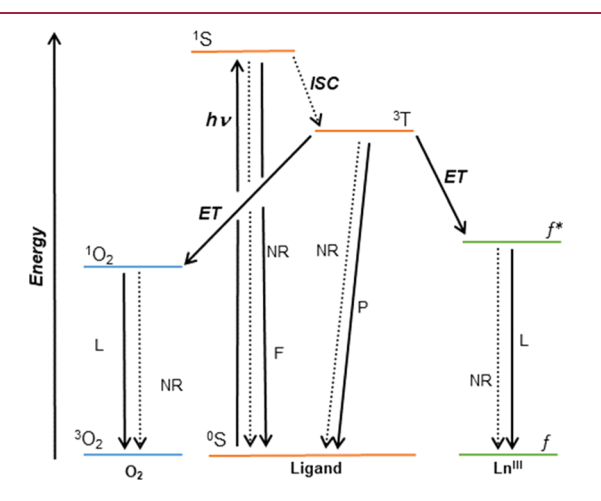


Figure 1. Simplified energy-level diagram illustrating the ET processes for $\operatorname{Ln^{III}}$ ion sensitization and ${}^{1}\operatorname{O}_{2}$ generation in this work. The ligand absorbs energy $h\nu$ to populate a singlet excited state (${}^{1}\operatorname{S}$). A triplet excited state (${}^{3}\operatorname{T}$) is formed after ISC. ${}^{3}\operatorname{T}$ can transfer energy to the emissive f^{*} excited state which decays by luminescence (L) to the ground state f or can lead to ${}^{1}\operatorname{O}_{2}$ generation. The decay of ${}^{1}\operatorname{O}_{2}$ to triplet oxygen ${}^{3}\operatorname{O}_{2}$ is seen through the emission at 1270 nm. Nonradiative (NR) pathways (dotted lines) can lead to the quenching of excited states. Other possible radiative processes are fluorescence (F) and phosphorescence (F). Energy levels are not drawn to scale.

Ln^{III}-based systems work well as multifunctional platforms with imaging capabilities, as recently demonstrated. ^{26–28} For example, a Tb^{III} DOTA-based complex that displays green Tb^{III}-centered emission with an efficiency of 24% and $^{\rm I}{\rm O}_2$ generation efficiency ($\phi_{^{\rm I}{\rm O}_2}$) of 12% was used to image NIH-3T3 cells. ²⁹ While this complex displayed efficient Tb^{III} luminescence, $\phi_{^{\rm I}{\rm O}_2}$ fell well below the efficiencies of organic photosensitizers. ³⁰ Patra and coworkers described Eu^{III} and Tb^{III} complexes which penetrate the cell membrane of H460 and MCF-7 cells. The IC₅₀ value of the more phototoxic Tb^{III} complex is 7.94 \pm 0.65 $\mu{\rm M}$ in H460 cells. The authors mention that the cells remained viable in the presence of the complexes in the dark. ³¹

Our group has described dually functional complexes with naphthalimide-containing antennae that sensitize visible-(Eu^{III}) and near-infrared (NIR)-emitting (Yb^{III}, Nd^{III}, and Er^{III}) ions in addition to generating $^1\text{O}_2$ with $\phi_{^1\text{O}_2}$ in the range 41–64%. These complexes are not water-soluble 32 and are

thus not viable for imaging and therapy applications in biological systems. More recently, we described a family of oligothiophene-based sensitizers of Ln^{III} emission, which show wavelength-dependent ${}^{1}O_{2}$ generation 33,34 but are also not water-soluble. Another series of oligothiophene-based ligands that were water-soluble were studied for their cytotoxicity toward HeLa cells. However, the latter displayed only weak Eu^{III}-centered luminescence due to two water molecules directly coordinated to the metal ion and were thus not useful for bioimaging.

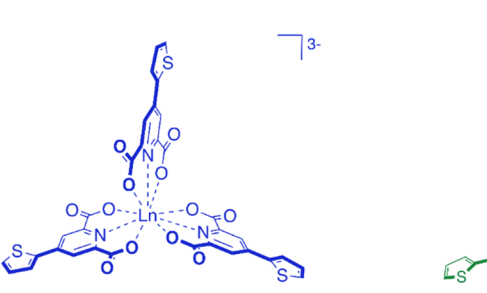
Oligothiophenes are naturally occurring plant pigments known for their ability to generate $^1\mathrm{O}_2$ with high $\phi_{^1\mathrm{O}_2}.^{^{30}}$ Because of this property, oligothiophenes and thienylderivatized compounds are reported to have applications as antiviral, anticancer, and antifungal agents. $^{36-38}$ Thus, thiophene-based functional groups are promising because of their ability to enhance ISC 39,40 and efficiently generate $^1\mathrm{O}_2$ and of their interesting photophysical properties. $^{33,34,42-46}$

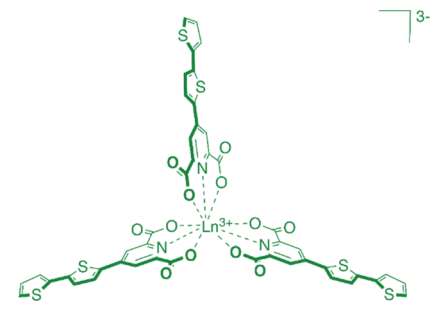
Dipicolinato-based compounds have been studied extensively for cell imaging.⁴⁷⁻⁵ Their usefulness can be attributed to the well-documented facile formation of the stable 3:1 ligand/metal complex, 52-57 which provides better shielding of the Ln^{III} from vibrational quenching in aqueous solution. Therefore, in pursuit of complexes with the dual properties of light emission and ¹O₂ generation, we coupled two moieties, a chelator capable of sensitizing Ln^{III}-based emission based on pyridine-bis(carboxylate) as well as a functional group capable of generating ¹O₂ based on thiophene or 2,2'-bithiophene, to generate new ligands that promote both properties when bound to Ln^{III} ions. The resulting 3:1 ligand-to-metal Ln^{III} ion complexes, shown in Scheme 1, are trianionic and watersoluble. We report here the synthesis and photophysical properties of the two new ligands, nTdpa2-, and their respective luminescent Ln^{III} ion complexes, $[Ln(nTdpa)_3]^{3-}$ $(n = 1 \text{ or } 2, Ln^{III} = Eu^{III}, Gd^{III}, \text{ or } Yb^{III})$. We show that [Eu(1Tdpa)₃]³⁻ is useful for cell fluorescence imaging and report the results of its colocalization studies, as well as the ¹O₂ generation ability, photocytotoxicity, and dark cytotoxicity of [Eu(1Tdpa)₃]³⁻ and the [Ln(2Tdpa)₃]³⁻ complexes in HeLa cells.

■ RESULTS AND DISCUSSION

 $\rm H_21Tdpa$ and $\rm H_22Tdpa$ were synthesized by Suzuki coupling thienyl- or bithienyl-functionalized borolane with brominated dipicolinic ester following a modified literature procedure (Scheme 2 and Supporting Information). Subsequent saponification of diethyl 4-(thiophen-2-yl)pyridine-2,6-dicarboxylate (n=1) or diethyl 4-(2,2'-bithiophen-5-yl)pyridine-2,6-dicarboxylate (n=2) led to the formation of $\rm H_21Tdpa$ and

Scheme 1. [Ln(1Tdpa)₃]³⁻ (Left) and [Ln(2Tdpa)₃]³⁻ (Right) Described Here





H₂2Tdpa

Scheme 2. Synthesis of H_2nTdpa (n = 1 or 2)

Table 1. Quantum Yields of Fluorescence (ϕ^F), Quantum Yields of Ln^{III} Luminescence (ϕ^{Ln}), and Ln^{III} Luminescence Lifetimes (τ_{Ln}) for [Ln(nTdpa)₃]³⁻ (n = 1 or 2) in Water (pH = 7.3) and Ethanol (Italicized Rows) at 25.0 \pm 0.1 °C^a

compound	$\phi^{ ext{F}}$ (%) no $ ext{Ln}^{ ext{III}}$	ϕ^{F} (%) Gd^{III}	$\phi^{ m Yb}$ (%)	φ ^{Eu} (%)	$ au^{ m Yb} \; (\mu m s)$	$ au^{ m Eu}~(m ms)$
$[Ln(1Tdpa)_3]^{3-}$	7 ± 1	3 ± 0	0.003 ± 0.000	33.3 ± 0.2	_d	1.15 ± 0.00 2.03 ± 0.00^{c}
$[Ln(2Tdpa)_3]^{3-}$	4 ± 1^{b} 28 ± 8 21 ± 1^{b}	6 ± 1^{b} 57 ± 4 55 ± 2^{b}	0.31 ± 0.00^{b} 0.0007 ± 0.0001 0.07 ± 0.00^{b}	41.0 ± 0.0^b	8.59 ± 0.01^{b} $\frac{d}{2}$ 9.76 ± 0.10^{b}	1.57 ± 0.00^b

^aLn^{III} = Gd^{III}, Yb^{III}, or Eu^{III}. ^bMeasured in 95% ethanol. ^cMeasured in D₂O. ^dYb^{III} emission is too low to reliably determine the lifetime.

 $\rm H_22Tdpa$ in 23% overall yield for both compounds. $\rm H_21Tdpa$ and $\rm H_22Tdpa$ were characterized using NMR spectroscopy and mass spectrometry (Figures S1–S4). To study the photophysical properties of these new compounds in aqueous solution, $\rm H_21Tdpa$ and $\rm H_22Tdpa$ were deprotonated with $\rm K_2CO_3$.

The Ln^{III} complexes were obtained by reacting solutions of K_2nTdpa with $LnCl_3$ ($Ln^{III} = Gd^{III}$, Eu^{III} , or Yb^{III}) in water and stirring at 50 °C for 24 h before spectroscopic characterization. The expected 3:1 ligand-to-metal stoichiometry of the complexes in solution, analogous to known dipicolinato complexes, 52-57 was confirmed through emission titration of K₂nTdpa with the YbCl₃ solution (Figures S5 and S6). The complexes were also characterized using mass spectrometry (Figures S7-S11) and elemental analysis showing results consistent with that stoichiometry. Emission lifetimes (vide infra) also confirm the saturation of the coordination sphere with the successful exclusion of water molecules, consistent with the 3:1 stoichiometry. For our studies, we isolated the complexes $K_3[Ln(nTdpa)_3]$ (n = 1 or 2 and $Ln^{III} = Eu^{III}$, Yb^{III} , or Gd^{III}) after solvent evaporation and redissolved them in the appropriate solvents.

The absorbance spectra of [1Tdpa]²⁻ and [2Tdpa]²⁻ in water are broad and structureless with maxima at 300 and 380 nm, respectively. The excitation spectra for both species match closely the respective absorbance spectra with maxima at 300

nm for the former and 364 nm for the latter (Figures S12–S16). The emission spectra display maxima at 380 nm ($\lambda_{\rm exc}$ = 300 nm) with an associated quantum yield of 7% and 464 nm ($\lambda_{\rm exc}$ = 360 nm) with a quantum yield of 28% for [1Tdpa]^{2–} and [2Tdpa]^{2–}, respectively (Table 1), and are similar to other thienyl-based compounds in water. ^{59,60} The fluorescence spectra of these compounds in 95% ethanol are virtually indistinguishable from those in water (Figures S15 and S16).

(5)

 $[\mathrm{Gd}(1\mathrm{Tdpa})_3]^{3-}$ and $[\mathrm{Gd}(2\mathrm{Tdpa})_3]^{3-}$ also fluoresce in the UV—vis region in water. When compared to the uncoordinated ligands, there are no considerable changes to the emission profiles (Figures S17 and S18). Fluorescence quantum yields (ϕ^F) , however, were 3 and 57%, respectively (Table 1). The latter is higher than the ϕ^F of the free ligand likely due to planarization of the ligand upon coordination to $\mathrm{Gd}^{\mathrm{III}}$ and some phosphorescence contribution due to improved ISC. ⁶¹ The fluorescence spectra in 95% ethanol show no appreciable change with respect to the potassium salts of the ligands (Table 1 and Figures S19 and S20).

In water, both ligands sensitize Yb^{III}, a NIR emitter, and the emission spectrum of $[Yb(1Tdpa)_3]^{3-}$ with the characteristic metal-centered ${}^2F_{5/2} \rightarrow {}^2F_{7/2}$ transition ($\lambda_{max} = 978$ nm) is seen when the complex is excited at 320 nm (Figure 2). A similar emission profile is seen when $[Yb(2Tdpa)_3]^{3-}$ is excited at 370 nm (Figure S21). Quantum yields of luminescence (ϕ^{Ln}) for both complexes were 0.003 and 0.0007% for

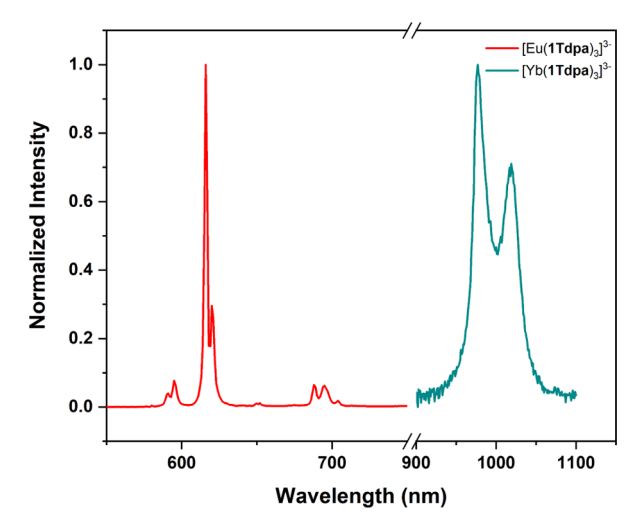


Figure 2. Normalized emission spectra of the $[Ln(1Tdpa)_3]^{3-}$ complex $[Ln^{III} = Eu^{III} \text{ (red) or Yb}^{III} \text{ (teal)}]$ in water at 25.0 \pm 0.1 $^{\circ}\text{C}$ (pH = 7.3); $[\text{complex}] = 5 \times 10^{-5} \text{ M}$; $\lambda_{\text{exc}} = 320 \text{ nm}$.

 $[Yb(1Tdpa)_3]^{3-}$ and $[Yb(2Tdpa)_3]^{3-}$, respectively, and are comparable to values for other luminescent Yb^{III} complexes in water. ⁶² Measurement of luminescence lifetimes were not reliable due to low signal intensity.

When exciting [Eu(1Tdpa)₃]³⁻ at 320 nm, the spectrum displays the characteristic Eu^{III}-centered transitions ${}^5D_0 \rightarrow {}^7F_I$ (J = 0-4) (Figure 2). The fine structure of the ${}^5D_0 \rightarrow {}^7F_2$ transition is consistent with a relatively low symmetry environment, distorted D_3 , around Eu^{III} 46,47,63 The efficiency of sensitized Eu^{III} emission (ϕ^{Eu}) was 33.3% in water (Table 1), which is more efficient than what is reported for the analogous dipicolinato complex ($\phi^{Eu} = 24\%^{52}$). Luminescence emission lifetimes (τ_{Eu}) were obtained in water and deuterated water and are 1.15 and 2.03 ms, respectively, and are similar to what is seen for other Eu^{III} complexes 47,64,65 (Figures S27 and S28 and Table S1). In both cases, these data fit a single exponential decay and are thus consistent with the presence of only one Eu^{III} species in solution. From the lifetimes in H₂O and D2O, we calculated the number of water molecules coordinated to Eu^{III}, q, in this complex; 66,67 the value of \sim 0 coordinated water molecules is consistent with a coordination environment composed of three $nTdpa^{2-}$ ligands. 66

Unlike what is observed for the Gd^{III} complexes and the ligands, the Ln^{III} luminescence properties are impacted by the change in solvent, as one would expect from the nature of the emitting species. The exchange of water for 95% ethanol reduces O-H quenching (Figures S24-S26), which results in an increase in ϕ^{Ln} (Table 1). Since the Yb^{III} luminescence increases in both complexes, we were able to measure au_{Yb} as 8.59 and 9.76 μ s for [Yb(1Tdpa)₃]³⁻ and [Yb(2Tdpa)₃]³⁻, respectively (Figures S30 and S31 and Table S2), which are similar to known complexes.^{68,69} Both lifetimes fit a single exponential decay consistent with a unique coordination environment around YbIII, and the similar values for both complexes indicate similar coordination geometries. The efficiencies $\phi^{\rm Yb}$, $\phi^{\rm Eu}$, $\tau^{\rm Eu}$, and $\phi^{\rm Eu}_{\rm Eu}$ also increase significantly when water is exchanged for 95% ethanol for $[Ln(1Tdpa)_3]^{3-}$ (Tables 1 and S3) again due to reduced quenching through O-H oscillators of the bulk solvent. It is important to note that the Eu^{III} emission profile remains the same, indicating that the symmetry around the metal center does not change as a result of changing solvent.⁶⁴

All compounds generate $^{1}O_{2}$, which was confirmed by the appearance of a phosphorescence peak at 1270 nm in the emission spectra (Figure S33). The $\phi_{^{1}O_{2}}$ for $^{2}Tdpa^{2-}$, $[Gd(1Tdpa)_{3}]^{3-}$, and $[Gd(2Tdpa)_{3}]^{3-}$ are 45, 13, and 23% in 95% ethanol, respectively (Table 2). It was not possible to

Table 2. Quantum Yields of Singlet Oxygen Generation ($\phi_{^{1}O_{2}}$) for $[\text{Ln}(n\text{Tdpa})_{3}]^{3-}$ (n=1 or 2) in 95% Ethanol at 25.0 \pm 0.1 °C

compound	no Ln ^{III}	Gd^{III}	$\mathrm{Eu}^{\mathrm{III}}$	Yb ^{III}
$[Ln(1Tdpa)_3]^{3-}$	LE	13 ± 0	LE	LE
$[Ln(2Tdpa)_3]^{3-}$	23 ± 0	45 ± 4		LE

 $^a\mathrm{LE}$ = $^1\mathrm{O}_2$ emission is observed but is too weak to reliably determine $\phi_{^1\mathrm{O}_2}.$

determine $\phi_{^{1}O_{2}}$ in some cases due to low phosphorescence intensity (Figure S32). Determination of $\phi_{^{1}O_{2}}$ was attempted in water, but due to the low dissolved O_{2} content (χ_{O2} in water = 0.2×10^{-4} , the phosphorescence signal was too weak to allow for reliable results (Figure S33). Nonetheless, the toxicity of these compounds was tested by incubating human cervical cancer carcinoma (HeLa) cells with the 2Tdpa $^{2-}$ -based compounds.

HeLa cells were selected for this study as they are an ideal candidate due to their robust characteristics. ⁷² Cell viability was assessed using an MTT metabolic activity assay in the dark and under UV light irradiation ($\lambda_{\rm exc}=365~{\rm nm}$). ⁷³ As shown in Figure 3a, the viability of HeLa cells decreases with increasing concentration of the photosensitizers when irradiated for 5 min. At most of the concentrations used, both Ln^{III} complexes, $[{\rm Gd}(2{\rm Tdpa})_3]^{3-}$ and $[{\rm Yb}(2{\rm Tdpa})_3]^{3-}$, are more photocytotoxic than $2{\rm Tdpa}^{2-}$. Control experiments show no appreciable change to cell viability within 5 min of irradiation, indicating that cell death is not observed in the absence of the photosensitizers.

HeLa cells were treated with the photosensitizers under the same conditions in the dark to test the compound's dark toxicity. Cell viability does not decrease below 80% for 3.00, 6.25, and 12.5 μ M (Figure 3b), and some dark cytotoxicity is observed at higher concentrations of 25 and 50 μM for all photosensitizers. IC₅₀ values in the dark and with irradiation were determined and are summarized in Table 3. Similar potencies for [Gd(2Tdpa)₃]³⁻ and [Yb(2Tdpa)₃]³⁻ are observed, and 2Tdpa²⁻ is notably less potent (Figure S36), which is likely due to the 3:1 ligand-to-metal stoichiometry of the complex. These $\rm IC_{50}$ values compare favorably to those of known photosensitizers. ^{74–76} The phototoxicity indices (PTIs) of the complexes (Table 3), after a short irradiation period of 5 min, compare favorably with those of reported photosensitizers, despite being lower than the values published for the most efficient ones. 15,17,18 The [Eu(1Tdpa)₃]³⁻ complex was also tested for cytotoxicity with HeLa cells when irradiated and in the dark (Figures S37 and S38). IC₅₀ determination showed that it is significantly less potent than the 2Tdpa²⁻derivatives (Table 3, Figure S39). This decrease in cytotoxicity is consistent with our observation of the low-intensity ¹O₂ emission at 1270 nm (Figure S32).

Although we do not anticipate leaching of the metal ion from these complexes, control experiments using the LnCl₃ salts were conducted and confirmed that the free metal ions are not cytotoxic (Figures S34–S38), as previously observed.³³

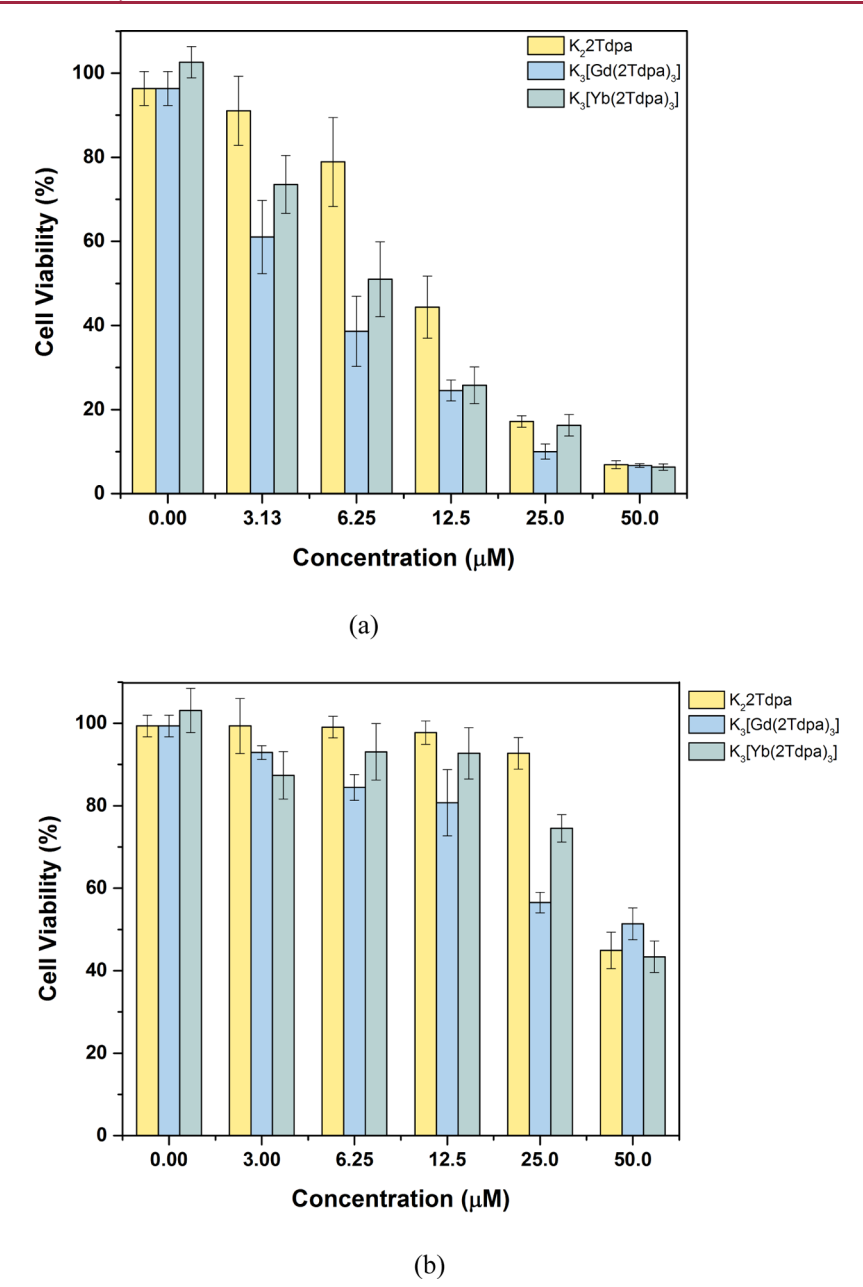


Figure 3. Cell viability (%, MTT assay) as a function of incubation concentration of 2Tdpa^{2-} (yellow) and $[\text{Gd}(2\text{Tdpa})_3]^{3-}$ (blue), or $[\text{Yb}(2\text{Tdpa})_3]^{3-}$ (green) (a) after 5 min of irradiation with 365 nm light and (b) in the dark. Control experiments were performed under the same experimental conditions.

The combined data suggest that these photosensitizers are potential photodynamic therapeutics with low dark toxicity.

The cell death mechanism was studied by flow cytometry of HeLa cells stained with Annexin V-fluorescein isothiocyanate (FITC) and propidium iodide (PI) after incubating the cells with 12.5 μM of the 2Tdpa²⁻-based compounds in the dark and after a short irradiation period of 5 min. Figure 4 shows the cell population of viable cells (FITC⁻/PI⁻), early-stage apoptotic cells (FITC⁺/PI⁻), late-stage apoptotic cells (FITC⁺/PI⁺), and necrotic cells (FITC⁻/PI⁺)⁷⁷ after treatment with 2Tdpa²⁻, [Gd(2Tdpa)₃]³⁻, or [Yb(2Tdpa)₃]³⁻. Cells treated with these compounds show minimal cell death in the dark (Figure 4a–c). However, when cells treated with these compounds are exposed to UV light, an increased percentage of cells indicate late apoptotic and necrotic processes. Cells incubated with 2Tdpa²⁻ (Figure 4d) are

26% necrotic and 16% apoptotic. In the dark, 91% of combined cells remain viable (Figure 4a). After irradiating with light, cells incubated with $[Gd(2Tdpa)_3]^{3-}$ are 44% necrotic and 28% apoptotic, yet less than 25% of combined cells show as necrotic or apoptotic when in the dark (Figure 4b,e). Likewise, cells incubated with $[Yb(2Tdpa)_3]^{3-}$ show 32% of cells as necrotic and 19% as late apoptotic in the light (Figure 4c,f). Figure S40 shows control experiments in the dark and under light irradiation, indicating that all cells remain viable in the absence of a photosensitizer.

These results indicate that 2Tdpa²⁻-mediated photolysis induces cell death by necrosis. PDT photosensitizers have been observed to trigger cell death by both necrosis and apoptosis and the latter is the most common pathway. ^{78,79} In fact, the cell death mechanism for the FDA-approved drug, Photofrin, when used in combination with carboplatin, shows significant

Table 3. IC_{50} Values and PTI for the $2Tdpa^{2-}$ -Based Compounds and $K_3[Eu(1Tdpa)_3]$ Compared to Known Photosensitizers

compound	$IC_{50}~(\mu M)~h\nu$	$IC_{50}~(\mu M)$ no $h \nu$	PTI
K ₂ 2Tdpa	10.5 ± 0.8	47.5 ± 2.5	4.5
$K_3[Gd(2Tdpa)_3]$	4.2 ± 0.5	39.7 ± 4.8	9.5
$K_3[Yb(2Tdpa)_3]$	6.3 ± 0.6	43.8 ± 3.6	7.0
$K_3[Eu(1Tdpa)_3]$	91.8 ± 5.1	435.3 ± 5.3	4.7
Photofrin ^a	7.1	>41	
Re-NH ₂ ^b	17.3 ± 2.9	>100	
[VO(cur)(phen)]Cl ^c	8.1 ± 0.3	>50	

"Data taken from ref 76; IC_{50} for this compound was expressed as 4.3 μ g/mL (light) and 25 μ g/mL (dark) in HeLa cells (MW: 605.7 g/mol) after 24 h incubation and irradiation with a broad-spectrum halogen lamp. ^bData taken from ref 74; IC_{50} for this compound was determined after 4 h incubation and irradiation with 350 nm light. ^cData taken from ref 75; cur = curcumin; phen = 1,10-phenanthroline; IC_{50} for this compound was determined after 4 h incubation and irradiation with a broad-spectrum source.

necrosis in HeLa cells. Onventionally, cell necrosis has been considered an unregulated process, which is independent of apoptosis. However, recent studies have demonstrated mechanisms with characteristics related to apoptosis and necrosis pathways. Although it is unclear to us why characteristics of both pathways have been observed, several

others have suggested that the balance between apoptosis and necrosis is dependent on multiple factors such as photosensitizer dose, cell type, genetic and metabolic potential, and the photosensitizers subcellular localization. 83–86

The promising luminescence properties of the Eu^{III} complex prompted us to evaluate its use as a luminescent dye for cellular imaging, including identifying its ability to permeate the cell membrane 79,84 and its subcellular location. Therefore, we incubated HeLa cells with 12.5 μ M of $[Eu(1Tdpa)_3]^{3-}$ (pH = 7.4), Hoechst 33342 (1 μ g/mL), and MitoTracker Green FM (50 nM) to determine cell permeability and subcellular localization. The live-cell images in Figure 5 show that Hoechst 33342 and Eu^{III} luminescence emission are observed when the cells are irradiated with 405 nm light (top center and right), and MitoTracker Green FM luminescence emission is observed when the cells are irradiated with 488 nm light (top left). The Eu^{III} compound appears to permeate the cell membrane of HeLa cells and co-localize in the same region as MitoTracker Green FM dye, indicating some cell specificity (bottom center).

Other Eu^{III} complexes which penetrate the membrane of HeLa cells were described by Yuan and coworkers who reported Eu^{III} complexes based on a derivative of 4'-(10-methyl-9-anthryl)-2,2':6',2"-terpyridine and display luminescence within HeLa cells, yet are weakly luminescent compared to the complex reported here ($\phi^{\text{Eu}} = 0.88\%$). ^{87,88} These

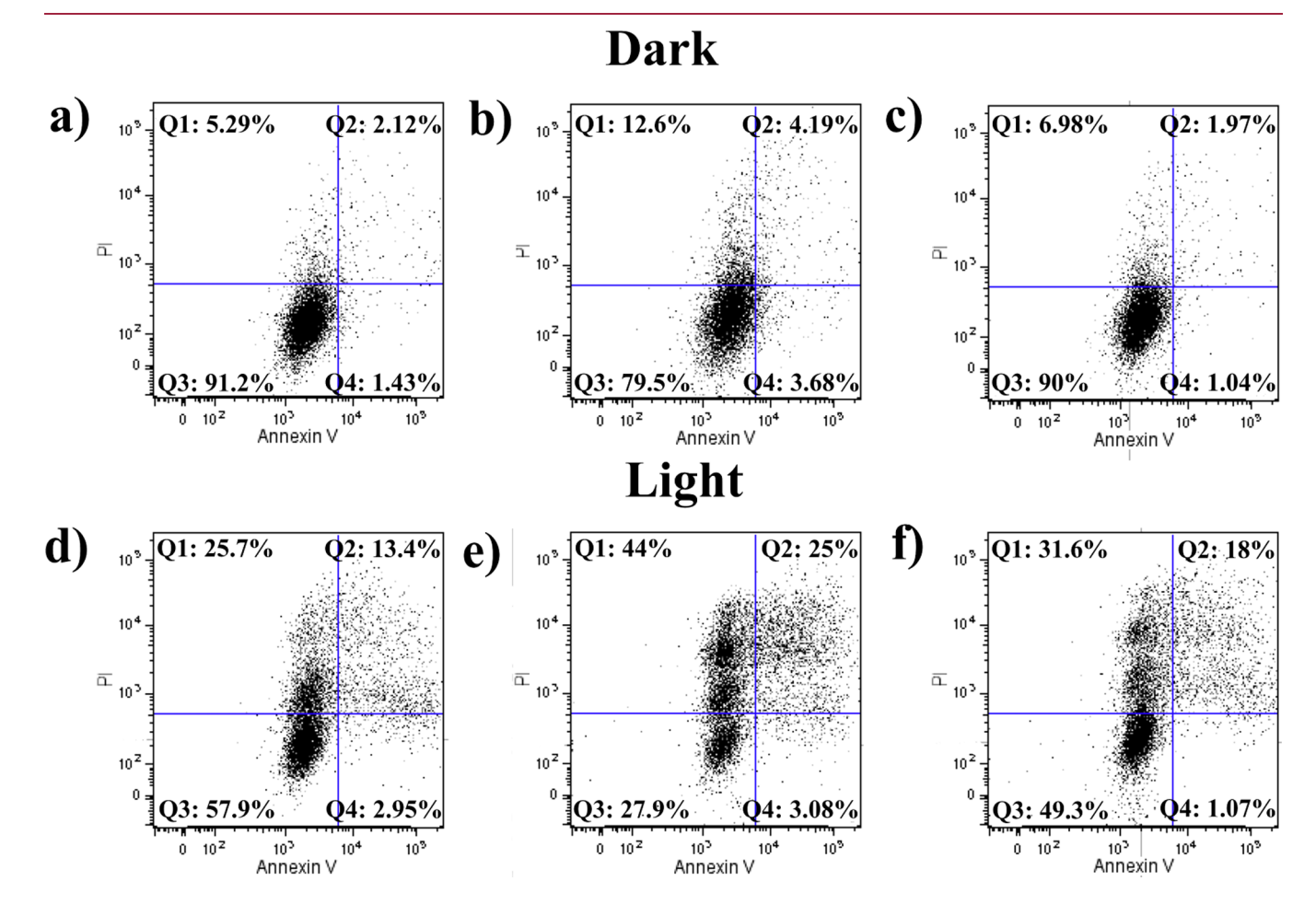


Figure 4. Flow cytometry quantification of HeLa cells stained with Annexin V-FITC and PI using $2Tdpa^{2-}$, $[Yb(2Tdpa)_3]^{3-}$, $[Gd(2Tdpa)_3]^{3-}$ as PDT sensitizers in the dark (a-c) and after light irradiation (d-f), respectively. Light/dark negative and light/dark positive controls were also examined (Figure S40).

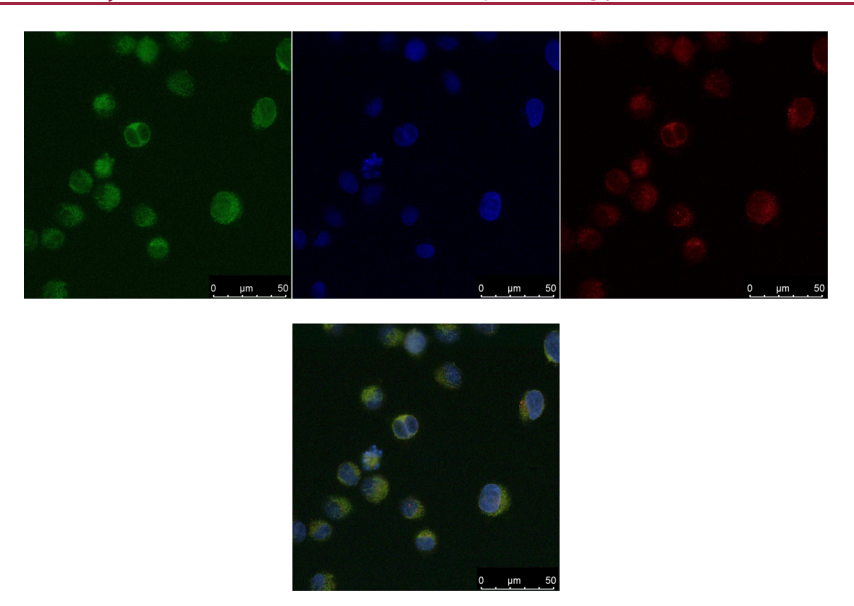


Figure 5. Live cell images of HeLa cells incubated with (top left) MitoTracker Green FM (50 nM, $\lambda_{\rm exc}$ = 488 nm), (top center) Hoechst 33342 (1 μ g/mL, $\lambda_{\rm exc}$ = 405 nm), (top right) [Eu(1Tdpa)₃]³⁻ (12 μ M, $\lambda_{\rm exc}$ = 405 nm), and (bottom center) merged image.

authors also characterized the complexes' photophysical properties in solution at high pH,⁸⁷ which is not near the pH of HeLa cells (7.9 ± 0.1^{89}) or within the typical pH range of animal cells $(6.5-7.5^{90})$. Chauvin, Bünzli, and coworkers reported a Eu^{III} complex based on a hexadentate bis-(benzimidazole)pyridine ligand with a quantum yield of 11% at pH = 7.4. Bioimaging of these complexes indicated cytoplasmic localization of HeLa cells. 91 Patra and coworkers synthesized Eu^{III} and Tb^{III} complexes with a dopaminefunctionalized diethylenetriaminepentaacetic acid ligand and reported ϕ^{Eu} and ϕ^{Tb} of 3.8 and 2.2%, respectively, at pH = 7.2. A high concentration (100 μ M) of each Ln^{III} complex for bioimaging, likely due to their poor luminescence efficiency, indicated cytoplasmic localization of the complexes within HeLa cells. In contrast, the luminescent Eu^{III} compound studied here efficiently sensitizes luminescence and coupled with its ability to generate ¹O₂ under irradiation (Figures S32, S37, and S39) provides a dual functionality that is absent from the above examples.

CONCLUSIONS

In summary, two thiophene-containing molecules were synthesized and used as sensitizers for $^1{\rm O}_2$ generation and Ln^{III} luminescence in the visible and NIR region. $^1{\rm O}_2$ generation was observed for all complexes discussed here, and the most efficient $^1{\rm O}_2$ generation was observed for the 2Tdpa $^{2-}$ -based compounds. These displayed photocytotoxicity toward HeLa cells after only a short irradiation period of 5 min and IC $_{50}$ values were determined and are in the range 4.2–10.5 $\mu{\rm M}$, while the IC $_{50}$ value for the red emissive [Eu(1Tdpa) $_3$] is 91.8 $\mu{\rm M}$. All compounds displayed low dark toxicity. [Eu(1Tdpa) $_3$] was further used as a luminescent dye for live-cell imaging, indicating that this compound penetrates the cell membrane where it localizes in the mitochondria.

These improved luminescence characteristics, water solubility, and photocytotoxicity toward HeLa cells make these compounds potentially interesting for PDT. As the pyridine-based ligands can be easily functionalized, while not discussed here, they serve as the basis for new compounds with improved characteristics, such as a red-shifted excitation wavelength, and

enhanced stability, in which the pyridine-based chelator shows higher denticity, as well as biocompatibility for diagnostic and therapeutic applications. Ultimately, our work shows that the targeted strategy of combining known cytotoxic compounds with chelators capable of sensitizing Ln^{III}-centered emission was successfully pursued and, as a strategy, should be viable for a variety of other systems as well.

■ EXPERIMENTAL SECTION

General Information. All the reagents used were of analytical grade, commercially obtained, and used as received. Solvents were dried by standard methods. The syntheses were completed under the N_2 atmosphere unless otherwise specified. The purity of the organic compounds and metal complexes was found to be at least 95% and was assessed by 1H NMR spectroscopy, high-resolution mass spectrometry (spectra in ESI), and combustion microanalysis where appropriate. Combustion microanalyses of the compounds used in the cytotoxicity studies were performed by Galbraith Laboratories (Knoxville, TN).

Synthesis of H₂n**Tdpa.** H₂n**T**dpa (n = 1 or 2) was synthesized as shown in Scheme 2.

Synthesis of Diethyl 4-Bromopyridine-2,6-dicarboxylate (1). This compound was synthesized using a modified literature procedure. The product was purified using a silica column and hexanes/ethyl acetate (1:1) as the eluent. The pure compound was isolated as a white powder. Yield: 2.0 g, 81%.

¹H NMR (CDCl₃, 400 MHz): 8.43 (s, py, 2H), 4.50 (q, CH₂, 4H), and 1.46 (t, CH₃, 6H) ppm.

Synthesis of 4,4,5,5-Tetramethyl-2-(thiophen-2-yl)-1,3,2-dioxaborolane (2). Potassium acetate (1.1 mg, 11 mmol), bis(pinacolato)-diboron (930 mg, 3.7 mmol), and $Pd(dppf)Cl_2$ (130 mg, 0.02 mmol) were added to a round-bottom flask containing dry toluene (10 mL) and heated to 80 °C for 24 h. The reaction was cooled and poured into water, and the product was extracted with diethyl ether (3 × 10 mL). The combined organic phases were washed with brine and dried over Na_2SO_4 . The solvent was removed under reduced pressure to yield yellow crystals. Yield: 730 mg, 94%.

¹H NMR (CDCl₃, 400 MHz): 7.66 (d, Th, 1H), 7.64 (d, Th, 1H), 7.19 (dd, Th, 1H), and 1.35 (s, CH₃, 12H) ppm.

Synthesis of Diethyl 4-(Thiophen-2-yl)pyridine-2,6-dicarboxylate (3). This compound was synthesized using a modified literature procedure. Section 2 (103 mg, 0.49 mmol), 1 (100 mg, 0.33 mmol), and XPhosPd G2 (26 mg, 0.033 mmol) were dissolved in deoxygenated tetrahydrofuran (THF) (2 mL). K₃PO₄ in deoxygenated water (1.4)

mL, 0.5 M) was added and stirred for 4 h at 50 °C. Distilled water (5 mL) was used to quench the reaction, and the product was extracted with CH_2Cl_2 (3 × 10 mL). The combined organic phases were dried over Na_2SO_4 and filtered, and the solvent was removed under reduced pressure. The product was purified using a silica column, with 1:1 hexanes/ethyl acetate as the eluent, and was isolated as light yellow crystals. Yield: 50 mg, 50%.

¹H NMR (CDCl₃, 400 MHz): 8.44 (s, py, 2H), 7.69 (d, Th, 1H), 7.69 (d, Th, 1H), 7.52 (d, Th, 1H), 7.19 (dd, Th, 1H), 4.52 (q, CH₂, 4H), and 1.48 (t, CH₃, 6H) ppm.

Synthesis of 4-(Thiophen-2-yl)pyridine-2,6-dicarboxylic Acid (H_2 1Tdpa). NaOH (45 mg, 1.1 mmol) was dissolved in distilled water (2 mL) and added dropwise to a solution of 3 (140 mg, 0.46 mmol) in 1:5 methanol/water (6 mL). The reaction was stirred at 60 °C for 4 h and cooled in an ice bath. HCl (1 M) was added until pH \sim 2, upon which an off-white precipitate formed. The precipitate was filtered, washed with cold water, and dried under low pressure. Yield: 16 mg, 61%.

¹H NMR (D₂O, 400 MHz): 8.32 (s, py, 2H), 8.01 (d, Th, 1H), 7.81 (d, Th, 1H), and 7.23 (dd, Th, 1H) ppm.

HR ESI-MS $(C_{11}H_6NO_4S)^-$: 248.0023 (calc), 248.0019 (exp).

Synthesis of 2-(2,2'-Bithiophen-5-yl)-4,4,5,5-tetramethyl-1,3,2-dioxaborolane (4). This compound was synthesized using a modified literature procedure. So N-Butyllithium (2.6 mL, 6.5 mmol, 2.5 M in hexane) was added dropwise to a chilled mixture of THF (50 mL) and 2,2'-bithiophene (1.0 g, 6.0 mmol) and stirred for 1 h at -78 °C. 2-Isopropoxy-4,4,5,5-tetramethyl-1,3,2-dioxaborolane (1.4 mL, 8.2 mmol) was added dropwise at -78 °C. The reaction was allowed to reach RT and stirred for an additional 20 h. Saturated NH₄Cl solution (20 mL) was used to quench the reaction, and the product was extracted with diethyl ether (3 × 15 mL). The combined organic phases were washed with water (3 × 10 mL) and brine (3 × 10 mL) and dried over Na₂SO₄. Excess solvent was removed under reduced pressure, and the product was purified using a silica column and 4:1 petroleum ether/ethyl acetate as the eluent. The pure product was isolated as a blue oil. Yield: 1.2 g, 69%.

¹H NMR (CDCl₃, 400 MHz): 7.53 (d, Th, 1H), 7.25 (d, Th, 1H), 7.23 (d, Th, 2H), 7.02 (t, Th, 1H), and 1.35 (s, CH₃, 12H) ppm.

Synthesis of Diethyl 4-(2,2'-Bithiophen-5-yl)pyridine-2,6-dicarboxylate (5). This compound was synthesized using a modified literature procedure. Set 4 (440 mg, 1.5 mmol), 1 (300 mg, 1 mmol), and XPhosPd G2 (78 mg, 0.1 mmol) were dissolved in deoxygenated THF (4 mL). K₃PO₄ in deoxygenated water (4.2 mL, 0.5 M) was added, and the reaction was stirred for 4 h at 50 °C. The reaction was quenched with water (5 mL), and the product was extracted with CH₂Cl₂ (3 × 10 mL). The combined organic phases were dried over Na₂SO₄ and filtered, and the solvent was removed under reduced pressure. The product was purified using a silica column, and 1:1 hexanes/ethyl acetate was used as the eluent. The product was isolated as green crystals. Yield: 210 mg, 54%.

¹H NMR (acetone-*d*₆, 400 MHz): 8.40 (s, py, 2H), 7.92 (d, Th, 1H), 7.54 (d, Th, 1H), 7.46 (d, Th, 1H), 7.40 (d, Th, 1H), 7.15 (t, Th, 1H), 4.45 (q, CH₂, 4H), and 1.42 (t, CH₃, 6H) ppm.

Synthesis of 4-(2,2'-Bithiophene)pyridine-2,6-dicarboxylic Acid (H₂ZTdpa). NaOH (45 mg, 1.1 mmol) was dissolved in distilled water (2 mL) and then added dropwise to a solution of 5 (150 mg, 0.39 mmol) in 1:5 methanol/water (6 mL). The reaction was stirred at 60 °C for 4 h and cooled in an ice bath. HCl (1 M) was added until pH ~ 2, forming a yellow precipitate. The product was filtered, washed with cold water, and dried under reduced pressure, yielding a yellow-brown powder. Yield: 930 mg, 76%.

¹H NMR (DMSO-*d*₆, 400 MHz): 9.87 (s, OH, 2 H), 8.16 (s, py, 2H), 7.86 (d, Th, 1H), 7.60 (d, Th, 1H), 7.46 (d, Th, 1H), 7.41 145 (d, Th, 1H), and 7.15 (t, Th, 1H) ppm.

ESI-MS $(C_{15}H_7KNO_4S_2)^-$: 367.9459 (calc), 367.9460 (exp).

Synthesis of K_2nTdpa (n=1 or 2). K_2CO_3 (0.5 mmol) and H_2nTdpa (n=1 or 2) (0.5 mmol) were dissolved in distilled water and stirred for 30 min, yielding colorless or yellow solutions for K_21Tdpa and K_22Tdpa , respectively. KOH and HCl were used, as appropriate, to adjust the pH to 7.2.

```
Elemental analysis calculated for K<sub>2</sub>1Tdpa: C, 40.60; H, 1.55; N, 4.30. Found: C, 40.40; H, 2.24; N, 3.65.
```

Elemental analysis calculated for $K_22Tdpa \cdot 2H_2O$: C, 40.62; H, 2.50; N, 3.16. Found: C, 40.15; H, 2.14; N, 2.64.

Synthesis of Lanthanide Complexes ($K_3[Ln(nTdpa)_3]$, n=1 or 2). All metal complexes were prepared by mixing 1 equiv of $LnCl_3$ ($Ln^{III} = Yb^{III}$, Gd^{III} , or Eu^{III}) with 3 equiv of K_21Tdpa or K_22Tdpa in water and stirred for 24 h at 50 °C.

```
K_3[Gd(1Tdpa)_3].
   Yield: 95%.
   [Gd(1Tdpa)_3]^{3-} + 2K^+.
   ESI-HRMS [C_{33}H_{215}GdK_2N_3O_{12}S_3]^- m/z: 976.8338 (calc),
976.8147 (exp) (Figure S8).
   K_3[Eu(1Tdpa)_3].
   Yield: 94%.
   [Eu(1Tdpa)_3]^{3-} + 2K^+.
   ESI-HRMS [C_{33}H_{215}EuK_2N_3O_{12}S_3]^- m/z: 971.8331 (calc),
971.8295 (exp) (Figure S7).
   Elemental analysis calculated for K<sub>3</sub>[Eu(1Tdpa)<sub>3</sub>]·6H<sub>2</sub>O: C, 35.42;
H, 2.43; N, 3.76. Found: C, 35.67; H, 1.93; N, 3.16.
   K_3[Yb(1Tdpa)_3].
   Yield: 91%.
   [Yb(1Tdpa)_3]^{3-} + 2H^+.
   ESI-HRMS [C_{33}H_{215}YbH_2N_3O_{12}S_3]^- m/z: 917.9168 (calc),
917.9208 (exp) (Figure S9).
   K_3[Gd(2Tdpa)_3].
   Yield: 98%.
   \begin{split} & [\text{Gd}(2\text{Tdpa})_3]^{3-} + \text{H}^+ + \text{K}^+. \\ & \text{ESI-HRMS} \  \, [\text{C}_{45}\text{H}_{224}\text{GdKN}_3\text{O}_{12}\text{S}_6]^- \  \  \textit{m/z} \text{:} \  \, 1184.8411 \  \  \, \text{(calc),} \end{split}
1184.8529 (exp) (Figure S10).
   Elemental analysis calculated for K<sub>3</sub>[Gd(2Tdpa)<sub>3</sub>]: C, 42.81; H,
1.68; N, 3.33. Found: C, 42.67; H, 2.02; N, 3.16.
   K_3[Yb(2Tdpa)_3].
   Yield: 91%.
   [Yb(2Tdpa)_3]^{3-} + 2H^+.
   ESI-HRMS [C_{45}H_{224}YbK_2N_3O_{12}S_6]^- m/z: 1162.9000 (calc),
1162.9177 (exp) (Figure S11).
   Elemental analysis calculated for K<sub>3</sub>[Yb(2Tdpa)<sub>3</sub>]·2H<sub>2</sub>O: C, 41.12;
H, 1.92; N, 3.20. Found: C, 41.02; H, 1.90; N, 3.06.
```

ASSOCIATED CONTENT

Supporting Information

The Supporting Information is available free of charge at https://pubs.acs.org/doi/10.1021/acs.jmedchem.0c01805.

Molecular formula strings, selected experimental details and instrument information, NMR and high-resolution mass spectra, speciation studies, absorption, excitation and emission spectra, emission lifetimes, efficiencies of light emission and singlet oxygen generation, cell viability studies, and IC_{50} values and flow cytometry experiments (PDF)

SMILES identifiers for developed compounds (CSV)

AUTHOR INFORMATION

Corresponding Author

Ana de Bettencourt-Dias — Department of Chemistry, University of Nevada, Reno, Reno, Nevada 89557, United States; oorcid.org/0000-0001-5162-2393; Email: abd@ unr.edu

Authors

Carime V. Rodrigues – Department of Chemistry, University of Nevada, Reno, Reno, Nevada 89557, United States; Laboratório de Inorgânica e Materiais, Instituto de Química, Universidade de Brasília, Brasilia 70910-900, Brazil

- Katherine R. Johnson Department of Chemistry, University of Nevada, Reno, Reno, Nevada 89557, United States;
 orcid.org/0000-0002-1323-0222
- Vincent C. Lombardi Department of Microbiology and Immunology, University of Nevada, Reno, Reno, Nevada 89557, United States
- Marcelo O. Rodrigues Laboratório de Inorgânica e Materiais, Instituto de Química, Universidade de Brasília, Brasilia 70910-900, Brazil
- Josiane A. Sobrinho Department of Chemistry, University of Nevada, Reno, Reno, Nevada 89557, United States

Complete contact information is available at: https://pubs.acs.org/10.1021/acs.jmedchem.0c01805

Author Contributions

¹C.V.M. and K.R.J. contributed equally to this manucript.

Notes

The authors declare no competing financial interest.

ACKNOWLEDGMENTS

The National Science Foundation (CHE-1800392 to AdBD) is gratefully acknowledged for financial support. Shanti Rawat and Prof. Jorge H.S.K. Monteiro are acknowledged for their support and guidance. Janina S. Ruprecht is acknowledged for collecting mass spectra. This work was carried out with support from the Coordination for the Improvement of Higher Education Personnel, (CAPES-Brazil) Process (88881.186961/2018-01 to CVSR-Capes Scholar—Brazil). Research reported in this publication used the Cellular and Molecular Imaging (CMI) core facility supported by the National Institute of General Medical Sciences of the National Institutes of Health under grant number P20 GM103650.

■ ABBREVIATIONS

¹O₂ singlet oxygen ¹S, singlet; ³T, triplet; DOTA, dodecane tetraacetic acid; dppf, diphenylphosphineferrocene; ET, energy transfer; exp, experimental; FITC, fluorescein isothiocyanate; ISC, inter-system crossing; L, luminescence; Ln^{III}, lanthanide-(III); MTT, 3-(4,5-dimethylthiazol-2-yl)-2,5-diphenyltetrazolium bromide; NIR, near-infrared; *n*Tdpa, oligo(*n*)thiophenefunctionalized dipicolinic acid; PDT, photodynamic therapy; PI, propidium iodide; PTI, phototoxicity index (while PI is the abbreviation commonly seen in the literature we use this one here to distinguish from propidium iodide); THF, tetrahydrofuran; XPhosPd G2, Buchwald second-generation Pd(0) catalyst.

REFERENCES

- (1) Hoye, A. T.; Davoren, J. E.; Wipf, P.; Fink, M. P.; Kagan, V. E. Targeting mitochondria. Acc. Chem. Res. 2008, 41, 87–97.
- (2) Ethirajan, M.; Chen, Y.; Joshi, P.; Pandey, R. K. The role of porphyrin chemistry in tumor imaging and photodynamic therapy. *Chem. Soc. Rev.* **2011**, *40*, 340–362.
- (3) Heinemann, F.; Karges, J.; Gasser, G. Critical overview of the use of Ru(II) polypyridyl complexes as photosensitizers in one-photon and two-photon photodynamic therapy. *Acc. Chem. Res.* **2017**, *50*, 2727–2736.
- (4) Monro, S.; Colón, K. L.; Yin, H.; Roque, J.; Konda, P.; Gujar, S.; Thummel, R. P.; Lilge, L.; Cameron, C. G.; McFarland, S. A. Transition metal complexes and photodynamic therapy from a tumor-centered approach: Challenges, opportunities, and highlights from the development of TLD1433. *Chem. Rev.* **2019**, *119*, 797–828.

- (5) Reynolds, T. Photodynamic therapy expands its horizons. *J. Natl. Cancer Inst.* **1997**, *89*, 112–114.
- (6) Kempa, M.; Kozub, P.; Kimball, J.; Rojkiewicz, M.; Kuś, P.; Gryczyński, Z.; Ratuszna, A. Physicochemical properties of potential porphyrin photosensitizers for photodynamic therapy. *Spectrochim. Acta, Part A* **2015**, *146*, 249–254.
- (7) Bonnett, R. Photosensitizers of the porphyrin and phthalocyanine series for photodynamic therapy. *Chem. Soc. Rev.* **1995**, *24*, 19–33.
- (8) Josefsen, L. B.; Boyle, R. W. Unique diagnostic and therapeutic roles of porphyrins and phthalocyanines in photodynamic therapy, imaging and theranostics. *Theranostics* **2012**, *2*, 916–966.
- (9) Dumoulin, F.; Durmuş, M.; Ahsen, V.; Nyokong, T. Synthetic pathways to water-soluble phthalocyanines and close analogs. *Coord. Chem. Rev.* **2010**, 254, 2792–2847.
- (10) Jiang, X.-J.; Lo, P.-C.; Tsang, Y.-M.; Yeung, S.-L.; Fong, W.-P.; Ng, D. K. P. Phthalocyanine—polyamine conjugates as pH-controlled photosensitizers for photodynamic therapy. *Chem.* —*Eur. J* **2010**, *16*, 4777—4783.
- (11) Lo, P.-C.; Huang, J.-D.; Cheng, D. Y. Y.; Chan, E. Y. M.; Fong, W.-P.; Ko, W.-H.; Ng, D. K. P. New amphiphilic silicon(IV) phthalocyanines as efficient photosensitizers for photodynamic therapy: Synthesis, photophysical properties, and in vitro photodynamic activities. *Chem. —Eur. J* **2004**, *10*, 4831–4838.
- (12) Dummin, H.; Cernay, T.; Zimmermann, H. W. Selective photosensitization of mitochondria in hela cells by cationic Zn(II)-phthalocyanines with lipophilic side-chains. *J. Photochem. Photobiol., B* **1997**, 37, 219–229.
- (13) O'Connor, A. E.; Gallagher, W. M.; Byrne, A. T. Porphyrin and nonporphyrin photosensitizers in oncology: Preclinical and clinical advances in photodynamic therapy. *Photochem. Photobiol.* **2009**, *85*, 1053–1074.
- (14) Potocny, A. M.; Pistner, A. J.; Yap, G. P. A.; Rosenthal, J. Electrochemical, spectroscopic, and ${}^{1}O_{2}$ sensitization characteristics of synthetically accessible linear tetrapyrrole complexes of palladium and platinum. *Inorg. Chem.* **2017**, *56*, 12703–12711.
- (15) Potocny, A. M.; Riley, R. S.; O'Sullivan, R. K.; Day, E. S.; Rosenthal, J. Photochemotherapeutic properties of a linear tetrapyrrole palladium(II) complex displaying an exceptionally high phototoxicity index. *Inorg. Chem.* **2018**, *57*, 10608–10615.
- (16) Wang, J.; Potocny, A. M.; Rosenthal, J.; Day, E. S. Gold nanoshell-linear tetrapyrrole conjugates for near infrared-activated dual photodynamic and photothermal therapies. *ACS Omega* **2020**, *5*, 926–940.
- (17) Sainuddin, T.; McCain, J.; Pinto, M.; Yin, H.; Gibson, J.; Hetu, M.; McFarland, S. A. Organometallic Ru(II) photosensitizers derived from *π*-expansive cyclometalating ligands: Surprising theranostic PDT effects. *Inorg. Chem.* **2016**, *55*, 83–95.
- (18) Soliman, N.; McKenzie, L. K.; Karges, J.; Bertrand, E.; Tharaud, M.; Jakubaszek, M.; Guérineau, V.; Goud, B.; Hollenstein, M.; Gasser, G.; Thomas, C. M. Ruthenium-initiated polymerization of lactide: A route to remarkable cellular uptake for photodynamic therapy of cancer. *Chem. Sci.* **2020**, *11*, 2657–2663.
- (19) Haxel, G. B.; Hedrick, J. B.; Orris, G. J. Rare Earth Elements-Critical Resources for High Technology, 2002.
- (20) Baskaran, R.; Lee, J.; Yang, S.-G. Clinical development of photodynamic agents and therapeutic applications. *Biomater. Res.* **2018**, 22, 25.
- (21) Schmitt, J.; Jenni, S.; Sour, A.; Heitz, V.; Bolze, F.; Pallier, A.; Bonnet, C. S.; Tóth, É.; Ventura, B. A porphyrin dimer—GdDOTA conjugate as a theranostic agent for one- and two-photon photodynamic therapy and MRI. *Bioconjugate Chem.* **2018**, *29*, 3726–3738.
- (22) Bünzli, J.-C. G. On the design of highly luminescent lanthanide complexes. *Coord. Chem. Rev.* **2015**, 293-294, 19–47.
- (23) Bünzli, J.-C. G.; Choppin, G. R. Lanthanide Probes in Life, Chemical and Earth Sciences-Theory and Practice; Elsevier: Amsterdam, 1989.
- (24) Bünzli, J.-C. G. Lanthanide luminescence for biomedical analyses and imaging. *Chem. Rev.* **2010**, *110*, 2729–2755.

- (25) de Bettencourt-Dias, A. Introduction to lanthanide ion luminescence. In *Luminescence of lanthanide ions in coordination compounds and nanomaterials*; de Bettencourt-Dias, A., Ed.; John Wiley & Sons, Ltd.: Chichester, United Kingdom, 2014, pp 1–48.
- (26) Dasari, S.; Singh, S.; Kumar, P.; Sivakumar, S.; Patra, A. K. Near-infrared excited cooperative upconversion in luminescent ytterbium(III) bioprobes as light-responsive theranostic agents. *Eur. J. Med. Chem.* **2019**, *163*, 546–559.
- (27) Jia, J.; Zhang, Y.; Zheng, M.; Shan, C.; Yan, H.; Wu, W.; Gao, X.; Cheng, B.; Liu, W.; Tang, Y. Functionalized Eu(III)-based nanoscale metal—organic framework to achieve near-ir-triggered and -targeted two-photon absorption photodynamic therapy. *Inorg. Chem.* **2018**, 57, 300—310.
- (28) Xu, F.; Zhao, Y.; Hu, M.; Zhang, P.; Kong, N.; Liu, R.; Liu, C.; Choi, S. K. Lanthanide-doped core—shell nanoparticles as a multimodality platform for imaging and photodynamic therapy. *Chem. Commun.* **2018**, *54*, 9525—9528.
- (29) Law, G.-L.; Pal, R.; Palsson, L. O.; Parker, D.; Wong, K.-L. Responsive and reactive terbium complexes with an azaxanthone sensitiser and one naphthyl group: Applications in ratiometric oxygen sensing in vitro and in regioselective cell killing. *Chem. Commun.* **2009**, 47, 7321–7323.
- (30) Redmond, R. W.; Gamlin, J. N. A compilation of singlet oxygen yields from biologically relevant molecules. *Photochem. Photobiol.* **1999**, *70*, 391–475.
- (31) Singh, K.; Goenka, A.; Ganesh, S.; Patra, A. K. Luminescent Eu^{III} and Tb^{III} complexes containing dopamine neurotransmitter: Biological interactions, antioxidant activity and cellular-imaging studies. *Eur. J. Inorg. Chem.* **2018**, *2018*, 3942–3951.
- (32) Johnson, K. R.; de Bettencourt-Dias, A. $^{1}O_{2}$ generating luminescent lanthanide complexes with 1,8-naphthalimide-based sensitizers. *Inorg. Chem.* **2019**, *58*, 13471–13480.
- (33) Johnson, K. R.; Vittardi, S. B.; Gracia-Nava, M. A.; Rack, J. J.; Bettencourt-Dias, A. Wavelength-dependent singlet oxygen generation in luminescent lanthanide complexes with a pyridine-bis-(carboxamide)-terthiophene sensitizer. *Chem.* —*Eur. J.* **2020**, *26*, 7274—7280.
- (34) Johnson, K. R.; Vittardi, S. B.; Gracia-Nava, M. A.; Rack, J. J.; de Bettencourt-Dias, A. Luminescent lanthanide complexes with a pyridine-bis(carboxamide)-bithiophene sensitizer showing wavelength-dependent singlet oxygen generation. *Dalton Trans.* **2020**, 49, 6661–6667.
- (35) Johnson, K. R.; Lombardi, V. C.; Bettencourt-Dias, A. Photocytotoxicity of oligothienyl-functionalized chelates that sensitize Ln^{III} luminescence and generate ¹O₂. *Chem. —Eur. J.* **2020**, 26, 12060–12066.
- (36) Hudson, J. B.; Harris, L.; Teeple, A.; Towers, G. H. N. The anti-HIV activity of the phytochemical α -terthienyl. *Antivir. Res.* **1993**, 20. 33–43.
- (37) Romagnoli, C.; Mares, D.; Fasulo, M. P.; Bruni, A. Antifungal effects of α -terthienyl from tagetes patula on five dermatophytes. *Phytother Res.* **1994**, *8*, 332–336.
- (38) Al-Said, M. S.; Bashandy, M. S.; Al-Qasoumi, S. I.; Ghorab, M. M. Anti-breast cancer activity of some novel 1,2-dihydropyridine, thiophene and thiazole derivatives. *Eur. J. Med. Chem.* **2011**, *46*, 137–141
- (39) Sadiq, F.; Zhao, J.; Hussain, M.; Wang, Z. Effect of thiophene substitution on the intersystem crossing of arene photosensitizers. *Photochem. Photobiol.* **2018**, *17*, 1794–1803.
- (40) Salzmann, S.; Kleinschmidt, M.; Tatchen, J.; Weinkauf, R.; Marian, C. M. Excited states of thiophene: Ring opening as deactivation mechanism. *Phys. Chem. Chem. Phys.* **2008**, *10*, 380–392.
- (41) Rangasamy, S.; Ju, H.; Um, S.; Oh, D.-C.; Song, J. M. Mitochondria and DNA targeting of 5,10,15,20-tetrakis(7-sulfonatobenzo[b]thiophene) porphyrin-induced photodynamic therapy via intrinsic and extrinsic apoptotic cell death. *J. Med. Chem.* **2015**, 58, 6864–6874.

- (42) de Bettencourt-Dias, A.; Poloukhtine, A. Phenylthiophene—dipicolinic acid-based emitters with strong solution blue and solid state green emission. *J. Phys. Chem. B* **2006**, *110*, 25638–25645.
- (43) de Bettencourt-Dias, A.; Viswanathan, S.; Rollett, A. Thiophene-derivatized Pybox and its highly luminescent lanthanide ion complexes. *J. Am. Chem. Soc.* **2007**, *129*, 15436–15437.
- (44) Hackbarth, S.; Pfitzner, S.; Guo, L.; Ge, J.; Wang, P.; Röder, B. Singlet oxygen kinetics in polymeric photosensitizers. *J. Phys. Chem. C* **2018**, *122*, 12071.
- (45) Hirai, Y.; Nakanishi, T.; Kitagawa, Y.; Fushimi, K.; Seki, T.; Ito, H.; Hasegawa, Y. Luminescent europium(III) coordination zippers linked with thiophene-based bridges. *Angew. Chem.* **2016**, *128*, 12238–12241.
- (46) Johnson, K. R.; Vittardi, S. B.; Gracia-Nava, M. A.; Rack, J. J.; de Bettencourt-Dias, A. Thiophene-derivatized pyridine-biscarbox-amide as a sensitizer for lniii luminescence and ¹O₂ generation. *J. Lumin.* **2020**, *49*, *6661*–*6667*.
- (47) Monteiro, J. H. S. K.; Machado, D.; de Hollanda, L. M.; Lancellotti, M.; Sigoli, F. A.; de Bettencourt-Dias, A. Selective cytotoxicity and luminescence imaging of cancer cells with a dipicolinato-based Eu^{III} complex. *Chem. Commun.* **2017**, *53*, 11818–11821.
- (48) Chauvin, A.-S.; Thomas, F.; Song, B.; Vandevyver, C. D. B.; Bünzli, J.-C. G. Synthesis and cell localization of self-assembled dinuclear lanthanide bioprobes. *Philos. Trans. R. Soc. A* **2013**, *371*, 20120295.
- (49) Gassner, A.-L.; Duhot, C.; Bünzli, J.-C.; Chauvin, A.-S. Remarkable tuning of the photophysical properties of bifunctional lanthanide tris(dipicolinates) and its consequence on the design of bioprobes. *Inorg. Chem.* **2008**, 47, 7802–7812.
- (50) Rajendran, M.; Miller, L. W. Evaluating the performance of time-gated live-cell microscopy with lanthanide probes. *Biophys. J.* **2015**, *109*, 240–248.
- (51) Eliseeva, S. V.; Auböck, G.; van Mourik, F.; Cannizzo, A.; Song, B.; Deiters, E.; Chauvin, A.-S.; Chergui, M.; Bünzli, J.-C. G. Multiphoton-excited luminescent lanthanide bioprobes: Two- and three-photon cross sections of dipicolinate derivatives and binuclear helicates. *J. Phys. Chem. B* **2010**, *114*, 2932–2937.
- (52) Chauvin, A.-S.; Gumy, F.; Imbert, D.; Bünzli, J.-C. G. Europium and terbium tris(dipicolinates) as secondary standards for quantum yield determination. [erratum to document cited in ca142:489604]. Spectrosc. Lett. 2007, 40, 193.
- (53) D'Aléo, A.; Picot, A.; Beeby, A.; Williams, J. A. G.; Le Guennic, B.; Andraud, C.; Maury, O. Efficient sensitization of europium, ytterbium, and neodymium functionalized tris-dipicolinate lanthanide complexes through tunable charge-transfer excited states. *Inorg. Chem.* **2008**, *47*, 10258–10268.
- (54) D'Aléo, A.; Picot, A.; Baldeck, P. L.; Andraud, C.; Maury, O. Design of dipicolinic acid ligands for the two-photon sensitized luminescence of europium complexes with optimized cross-sections. *Inorg. Chem.* **2008**, *47*, 10269–10279.
- (55) Monteiro, J. H. S. K.; Fetto, N. R.; Tucker, M. J.; de Bettencourt-Dias, A. Complexes with high two-photon absorption cross-section enable viscosity-sensing in the visible and near IR with one- and two-photon excitation. *Inorg. Chem.* **2020**, *59*, 3193–3199.
- (56) Chauvin, A. S.; Gumy, F.; Imbert, D.; Bünzli, J. C. G. Europium and terbium tris(dipicolinates) as secondary standards for quantum yield determination. *Spectrosc. Lett.* **2004**, *37*, 517–532.
- (57) Monteiro, J. H. S. K.; Sigoli, F. A.; de Bettencourt-Dias, A. A water-soluble Tb^{III} complex as temperature-sensitive luminescent probe. *Can. J. Chem.* **2018**, *96*, 859–864 invited to special issue of the Electron Donor-Accepter Interactions Gordon Research Conference.
- (58) Gabrielsson, E.; Tian, H.; Eriksson, S. K.; Gao, J.; Chen, H.; Li, F.; Oscarsson, J.; Sun, J.; Rensmo, H.; Kloo, L.; Hagfeldt, A.; Sun, L. Dipicolinic acid: A strong anchoring group with tunable redox and spectral behavior for stable dye-sensitized solar cells. *Chem. Commun.* **2015**, *51*, 3858–3861.

- (59) Poirel, A.; Retailleau, P.; De Nicola, A.; Ziessel, R. Synthesis of water-soluble red-emitting thienyl-bodipys and bovine serum albumin labeling. *Chem. —Eur. J.* **2014**, *20*, 1252–1257.
- (60) Mørkved, E. H.; Afseth, N. K.; Zimcik, P. Azaphthalocyanines with extended conjugation through heteroaryl and aryl substituents: Photochemical and photophysical properties. *J. Porphyr. Phthalocyanines* **2007**, *11*, 130–138.
- (61) Ko, C.-C.; Yam, V. W.-W. Coordination compounds with photochromic ligands: Ready tunability and visible light-sensitized photochromism. *Acc. Chem. Res.* **2018**, *51*, 149–159.
- (62) Werts, M. H. V.; Verhoeven, J. W.; Hofstraat, J. W. Efficient visible light sensitisation of water-soluble near-infrared luminescent lanthanide complexes. *Perkin 1* **2000**, *2*, 433–439.
- (63) Johnson, K. R.; de Bettencourt-Dias, A. Azido- and aminosubstituted dipicolinates for the sensitization of the luminescent lanthanides Eu^{III} and Tb^{III}. *Inorg. Chim. Acta* **2021**, *514*, 120003.
- (64) Aebischer, A.; Gumy, F.; Bünzli, J.-C. G. Intrinsic quantum yields and radiative lifetimes of lanthanide tris(dipicolinates). *Phys. Chem. Chem. Phys.* **2009**, *11*, 1346–1353.
- (65) Mohamadi, A.; Miller, L. W. Brightly luminescent and kinetically inert lanthanide bioprobes based on linear and preorganized chelators. *Bioconjugate Chem.* **2016**, 27, 2540–2548.
- (66) Supkowski, R. M.; Horrocks, W. D. On the determination of the number of water molecules, q, coordinated to europium(III) ions in solution from luminescence decay lifetimes. *Inorg. Chim. Acta* **2002**, 340, 44–48.
- (67) Horrocks, W. D.; Sudnick, D. R. Lanthanide ion luminescence probes of the structure of biological macromolecules. *Acc. Chem. Res.* **1981**, *14*, 384–392.
- (68) Zhang, Z.; Zhou, Y.; Li, H.; Gao, T.; Yan, P. Visible light sensitized near-infrared luminescence of ytterbium via ilct states in quadruple-stranded helicates. *Dalton Trans.* **2019**, *48*, 4026.
- (69) Wang, Y.-G.; Li, Y.-Q.; Tang, H.-H.; Lin, L.-R.; Ma, L.-H. Near-infrared photoluminescence and reversible trans-to-cis photoisomerization of mononuclear and binuclear ytterbium(III) complexes functionalized by azobenzene groups. ACS Omega 2018, 3, 5480—5490.
- (70) Ramesh, H.; Mayr, T.; Hobisch, M.; Borisov, S.; Klimant, I.; Krühne, U.; Woodley, J. M. Measurement of oxygen transfer from air into organic solvents. *J. Chem. Technol. Biotechnol.* **2016**, *91*, 832–836.
- (71) Sato, T.; Hamada, Y.; Sumikawa, M.; Araki, S.; Yamamoto, H. Solubility of oxygen in organic solvents and calculation of the hansen solubility parameters of oxygen. *Ind. Eng. Chem. Res.* **2014**, *53*, 19331–19337.
- (72) Lucey, B. P.; Nelson-Rees, W. A.; Hutchins, G. M. Henrietta Lacks, HeLa cells, and cell culture contamination. *Arch. Pathol. Lab Med.* **2009**, *133*, 1463–1467.
- (73) van Meerloo, J.; Kaspers, G. J. L.; Cloos, J. Cell sensitivity assays: The MTT assay. In *Cancer cell culture: Methods and protocols*; Cree, I. A., Ed.; Humana Press: Totowa, NJ, 2011, pp 237–245.
- (74) Leonidova, A.; Pierroz, V.; Rubbiani, R.; Heier, J.; Ferrari, S.; Gasser, G. Towards cancer cell-specific phototoxic organometallic rhenium(I) complexes. *Dalton Trans.* **2014**, *43*, 4287–4294.
- (75) Banerjee, S.; Prasad, P.; Hussain, A.; Khan, I.; Kondaiah, P.; Chakravarty, A. R. Remarkable photocytotoxicity of curcumin in hela cells in visible light and arresting its degradation on oxovanadium(IV) complex formation. *Chem. Commun.* **2012**, *48*, 7702–7704.
- (76) Delaey, E.; van Laar, F.; De Vos, D.; Kamuhabwa, A.; Jacobs, P.; de Witte, P. A comparative study of the photosensitizing characteristics of some cyanine dyes. *J. Photochem. Photobiol., B* **2000**, *55*, 27–36.
- (77) Lv, Z.; Zou, L.; Wei, H.; Liu, S.; Huang, W.; Zhao, Q. Phosphorescent starburst Pt(II) porphyrins as bifunctional therapeutic agents for tumor hypoxia imaging and photodynamic therapy. *ACS Appl. Mater. Interfaces* **2018**, *10*, 19523–19533.
- (78) Oleinick, N. L.; Evans, H. H. The photobiology of photodynamic therapy: Cellular targets and mechanisms. *Radiat. Res.* **1998**, *150*, S146–S156.

- (79) Castano, A. P.; Demidova, T. N.; Hamblin, M. R. Mechanisms in photodynamic therapy: Part one—photosensitizers, photochemistry and cellular localization. *Photodiagnosis Photodyn. Ther.* **2004**, *1*, 279–293
- (80) Choi, Y.; Chang, J. E.; Jheon, S.; Han, S. J.; Kim, J. K. Enhanced production of reactive oxygen species in hela cells under concurrent low-dose carboplatin and photofrin photodynamic therapy. *Oncol. Rep.* **2018**, *40*, 339–345.
- (81) Hail, N.; Carter, B. Z.; Konopleva, M.; Andreeff, M. Apoptosis effector mechanisms: A requiem performed in different keys. *Apoptosis* **2006**, *11*, 889–904.
- (82) Soriano, J.; Villanueva, A.; Stockert, C. J.; Cañete, M. Regulated necrosis in HeLa cells induced by ZnPc photodynamic treatment: A new nuclear morphology. *Int. J. Mol. Sci.* **2014**, *15*, 22772.
- (83) Piette, J.; Volanti, C.; Vantieghem, A.; Matroule, J.-Y.; Habraken, Y.; Agostinis, P. Cell death and growth arrest in response to photodynamic therapy with membrane-bound photosensitizers. *Biochem. Pharmacol.* **2003**, *66*, 1651–1659.
- (84) Castano, A. P.; Mroz, P.; Hamblin, M. R. Photodynamic therapy and anti-tumour immunity. *Nat. Rev. Cancer* **2006**, *6*, 535–545
- (85) Fabris, C.; Valduga, G.; Miotto, G.; Borsetto, L.; Jori, G.; Garbisa, S.; Reddi, E. Photosensitization with zinc(II) phthalocyanine as a switch in the decision between apoptosis and necrosis. *Cancer Res.* **2001**, *61*, 7495.
- (86) Yoo, J.-O.; Lim, Y.-C.; Kim, Y.-M.; Ha, K.-S. Differential cytotoxic responses to low-and high-dose photodynamic therapy in human gastric and bladder cancer cells. *J. Cell Biol.* **2011**, *112*, 3061–3071
- (87) Dai, Z.; Tian, L.; Xiao, Y.; Ye, Z.; Zhang, R.; Yuan, J. A cell-membrane-permeable europium complex as an efficient luminescent probe for singlet oxygen. *J. Mater. Chem. B* **2013**, *1*, 924–927.
- (88) Song, B.; Wang, G.; Tan, M.; Yuan, J. A europium(III) complex as an efficient singlet oxygen luminescence probe. *J. Am. Chem. Soc.* **2006**, *128*, 13442–13450.
- (89) Llopis, J.; McCaffery, J. M.; Miyawaki, A.; Farquhar, M. G.; Tsien, R. Y. Measurement of cytosolic, mitochondrial, and golgi ph in single living cells with green fluorescent proteins. *Proc. Natl. Acad. Sci. U.S.A.* 1998, 95, 6803–6808.
- (90) Roos, A.; Boron, W. F. Intracellular pH. *Physiol. Rev.* **1981**, *61*, 296–434.
- (91) Chauvin, A.-S.; Comby, S.; Song, B.; Vandevyver, C. D. B.; Thomas, F.; Bünzli, J.-C. G. A polyoxyethylene-substituted bimetallic europium helicate for luminescent staining of living cells. *Chem. Eur. J.* **2007**, *13*, 9515–9526.
- (92) Kleoff, M.; Suhr, S.; Sarkar, B.; Zimmer, R.; Reissig, H. U.; Marin-Luna, M.; Zipse, H. Efficient syntheses of new super Lewis basic tris(dialkylamino)-substituted terpyridines and comparison of their methyl cation affinities. *Chem. —Eur. J.* **2019**, 25, 7526–7533.